

Rotating Magnetocaloric Effect in First-order Phase Transition Material $\text{Gd}_5\text{Si}_2\text{Ge}_2$

Rafael Almeida^a, Rodrigo Kiefe^b, Ricardo Moura Costa Pinto^a, João Sequeira Amaral^b, Kyle Dixon-Anderson^{c,d}, Yaroslav Mudryk^{c,d}, João Pedro Araújo^a and João Horta Belo^{a,*}

^aIFIMUP – Institute of Physics for Advanced Materials, Nanotechnology and Photonics, Department of Physics and Astronomy, Faculty of Sciences of University of Porto, Rua do Campo Alegre, 687, 4169-007 Porto, Portugal

^bPhysics Department and CICECO — Aveiro Institute of Materials, University of Aveiro, 3810-193 Aveiro, Portugal

^cDivision of Materials Science and Engineering, Ames Laboratory of US DOE, Iowa State University, Ames, Iowa 50011-3020, United States

^dDepartment of Materials Science and Engineering, Iowa State University, Ames, Iowa 50011-2300, United States

ARTICLE INFO

Keywords:
magnetocaloric effect
magnetic refrigeration
demagnetizing effect

ABSTRACT

The rotating magnetocaloric effect (RMCE) induced by self-demagnetization has been investigated in the giant magnetocaloric effect (GMCE) material $\text{Gd}_5\text{Si}_2\text{Ge}_2$. This shape-dependent effect had thus far only been reported in pure Gd, marking this as the first analysis of the effect in a sample with a magnetostructural first-order phase transition. By rotating the applied magnetic field vector while keeping its intensity constant, the demagnetizing field within a high-aspect ratio sample changes significantly, resulting in a RMCE. We characterize RMCE by determining the adiabatic temperature change (ΔT_{ad}^{rot}) directly through temperature measurements, and the isothermal entropy change (ΔS_M^{rot}) via magnetometry and magnetostatic simulations. We obtain a remarkable maximum ΔT_{ad}^{rot} of 1.77 K for a constant external field of 0.8 T, higher than that obtained under 1.0 T. The magnetostatic simulations not only corroborate the highly non-monotonous field-dependence of $|\Delta S_M^{rot}|$, which reaches 95% of its maximum value at 0.8 T, $6.12 \text{ J K}^{-1} \text{ kg}^{-1}$ for the experimentally measured shape, but also estimate a 35% increase in the maximum $|\Delta S_M^{rot}|$ up to $8.67 \text{ J K}^{-1} \text{ kg}^{-1}$ in a simulated shape with higher aspect ratio.

1. Introduction

The magnetocaloric effect (MCE) has been intensely investigated in the past three decades due to its potential application in highly efficient heat pumps without vapor refrigerants [1, 2, 3, 4, 5].

Although the MCE has been known as a basic property of magnetic materials for over 100 years [6, 7], it was not considered for room temperature refrigeration until 1976, when G. Brown reported a device capable of generating a 47 K temperature span in a water-ethanol mixture with gadolinium [8, 9]. Two years later, in a report that went unpublished until 2014 [10], G. Brown and S. S. Papell showed that the same device was capable of generating an 80 K temperature span by increasing the amount of Gd used and improving other components to decrease fluid mixture.

The interest in the MCE was renewed around three decades ago with the discovery of alloys displaying magnetostructural first-order phase transitions (FOPT) that lead to a giant magnetocaloric effect (GMCE) at room temperature, nearly double the peak intensity of the MCE in Gd, which displays a magnetic second-order phase transition (SOPT) [11, 12]. Since then, several other prominent material families with GMCE near ambient temperature have been discovered and optimized, such as La-Fe-Si, Mn-Fe-P-Si, Ni-Mn-In, and others [13, 14, 15, 16].

This study focuses on one of the first-order phase transition materials exhibiting a GMCE - $\text{Gd}_5\text{Si}_2\text{Ge}_2$. It is part of the larger family of alloys, $\text{Gd}_5(\text{Si}_x\text{Ge}_{1-x})_4$, with varying properties and phase transition temperatures between 40 K ($x=0$) and 340 K ($x=1$) [12, 17].

With few exceptions, RMCE has been mainly studied in single-crystals or textured polycrystals with magneto-crystalline anisotropy (MCA) [18, 19, 20]. Despite the wide recognition of the relevance of the demagnetizing effect to the MCE [21, 22, 23, 24, 25], few studies demonstrate its potential to generate a RMCE by rotating a high aspect-ratio sample within a constant magnetic field. The first to accomplish this was a patent published by J. Barclay et al. in 1984, where an adiabatic temperature change (ΔT_{ad}) induced by external field rotation (ΔT_{ad}^{rot}) is presented in a Gd sample under a constant magnetic field of 0.3 T. Recently, a 2023 study featured an analogous experiment for a Gd sample

*Corresponding author: jbelo@fc.up.pt
ORCID(s):

rotating under a higher magnetic field (1.6 T) and finally, in early 2024, a detailed magnetic field-dependent study revealed the highly non-monotonous field-dependence of the demagnetizing field-induced RMCE in Gd [26, 27, 28].

One of the main challenges for mass adoption of magnetic refrigeration systems is the cost of generating magnetic field. The permanent magnet structures used are often the most expensive part of the devices [29], and the work required to alternate the magnetic field value on the magnetocaloric material to induce an MCE can represent over 50% of the total input power [30]. To modulate the magnetic field intensity, conventional magnetic refrigeration systems cyclically shift parts of the permanent magnet structures, or move the magnetocaloric material from high to low magnetic field zones [31, 32]. On the other hand, a system based on the RMCE only requires a change in the magnetic field orientation, so the magnetocaloric material may remain inside a high magnetic field zone throughout the thermodynamic process. Furthermore, the above-mentioned magnetic field-dependent study revealed that the RMCE of Gd was most competitive with the conventional MCE when using low magnetic field intensities, which is also a way of significantly reducing the amount of permanent magnet material required [28]. This suggests that RMCE could be a viable alternative basis for magnetic refrigeration devices that aim to use low magnetic field intensities.

While the rich physics of $\text{Gd}_5\text{Si}_2\text{Ge}_2$ have already been extensively studied since its discovery in 1997 [33, 34, 35], the current work is the first to measure and extensively characterize RMCE induced by the demagnetizing effect in this or any other FOPT GMCE material.

2. Methods and experimental details

We characterize RMCE of $\text{Gd}_5\text{Si}_2\text{Ge}_2$ as a function of sample temperature and external field amplitude in two complementary approaches: direct measurements of temperature to determine ΔT_{ad} and ΔT_{ad}^{rot} , and magnetometry to determine the isothermal entropy change on field application (ΔS_M). Magnetometry is then complemented with simulations from the 3D finite element magnetostatics simulation software *FEMCE* (Finite Element Magnetocaloric Effect) [36] to enable the determination of the isothermal entropy change on field rotation ΔS_M^{rot} . The direct measurements were done with an applied magnetic field up to 1.0 T, while the magnetometry study was done up to 2.0 T.

2.1. Sample preparation

A 6 g button of $\text{Gd}_5\text{Si}_2\text{Ge}_2$ was prepared through arc-melting, using high-purity gadolinium metal from the Materials Preparation Center of the Ames National Laboratory. Ge and Si were commercially sourced. The weight losses during melting were less than 1 wt.%. The sample was annealed to improve homogeneity. Magnetic and structural characterization confirmed the intended phase was manufactured and can be found in appendix A.

For the study of the demagnetizing field-induced RMCE, a high aspect-ratio shape is required so that the demagnetizing field is substantially different when the applied field is oriented along different directions, and a significant change in internal field may be induced by rotation [28]. To this end, the approximately ellipsoid shape of the cast button of the sample was cut in half, such that the region with the widest cross-section was accessed. Then, the thickness was reduced to 1.8 mm. For maximizing the demagnetizing field-based RMCE, a narrower sample would be beneficial (this is explored further ahead), but the brittle nature of the alloy would make it susceptible to breaking during shaping or measurements. The final sample weighed 628.3 mg, and its shape can be seen in figure 1.

2.2. Direct temperature measurements

To measure the sample temperature upon magnetic field changes, a type-K thermocouple with 25 μm -diameter wire was used. Typically, the thermocouple sensing tip is sandwiched between two halves of the sample, allowing a remarkably fast time-response [37], but this would decrease its overall aspect ratio. Instead, a similar effect was achieved while keeping the sample thickness as low as possible by using a negligible amount (less than 1 mg) of aluminium foil to press the thermocouple tip against the sample, removing excess adhesive (GE-varnish), and fully surrounding the thermocouple tip, improving thermal contact without compromising the demagnetizing field-based RMCE (see figure 1(h)).

The sample was mounted in a closed-circuit cryostat under vacuum ($P < 10^{-4}$ mbar). Two thin layers of craft paper acted as a thermal resistance to slow down the heat exchange between the sample and the copper base, further improving adiabatic conditions. The field source is an electromagnet for field intensities between 0.2 T and 0.8 T, or a Halbach array of permanent magnets for 1.0 T. For field applications/removals, the magnetic field source is physically moved such that the sample is inserted and removed from the magnetized region in less than 1 second. For the field

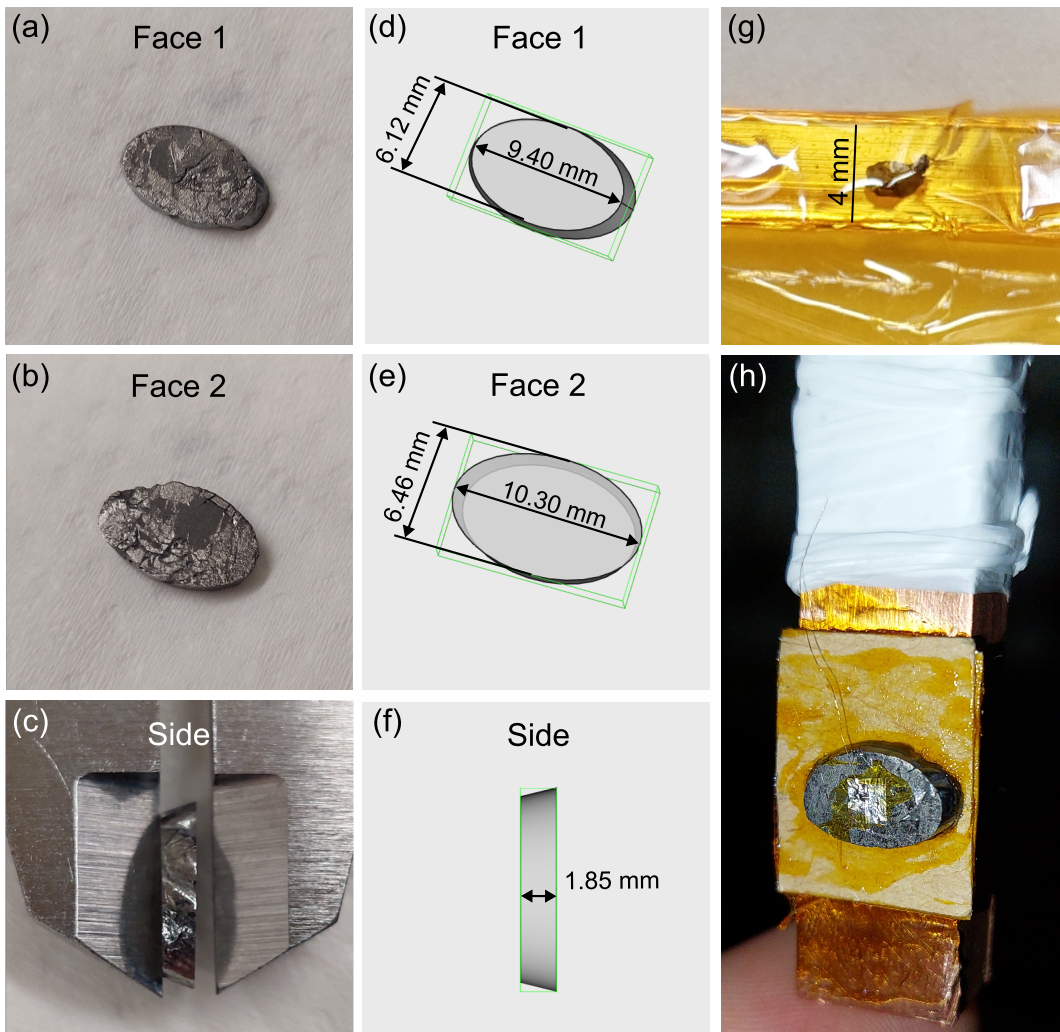


Figure 1: Photos of the sample used for direct temperature measurements (a-c) and corresponding pictures of the CAD 3D model used for the magnetostatic simulations (d-f). (g) The smaller sample measured in the MPMS, mounted on a quartz sample holder with polyimide tape. (h) The sample mounted on the cryostat, with thermocouple installed.

rotations, the sample is constantly in the magnetized region. The Halbach array is rotated in less than 1 second, and the electromagnet in about 2 seconds. These time intervals are only about 4% of the thermal exchange time-constant (45 s), such that an exponentially decaying temperature would only be underestimated by 5% (see figure 2). Temperature acquisition and control was done with a *Lakeshore 336* temperature controller.

The thermocouple's signal noise level is 0.02 K, making data processing the determining factor for uncertainty. Namely, how much time is given for thermal equilibrium to occur after a field change. Choosing between reasonable variations of that time (2 ± 1 s) results in a maximum variation of the obtained ΔT_{ad} below ± 0.1 K, which is below 10% for most of the presented measurements.

Details on the measurement protocols are given in the results section.

2.3. Magnetometry

A smaller, irregularly shaped fragment with $m = 6.93$ mg picked from the same cast button (see figure 1(g)) was used for the magnetization measurements. The *MPMS3* commercial SQUID magnetometer was used to measure magnetization versus temperature and magnetic field. The absolute values measured were corrected following the geometry-independent procedure described in reference [38].

2.4. Isothermal entropy change calculation

The determination of ΔS_M from magnetization measurements is done through the numerical integration of the Maxwell relation

$$\Delta S_M(T, H_f, H_i) = \mu_0 \int_{H_i}^{H_f} \frac{\partial M(T, H)}{\partial T} dH. \quad (1)$$

However, the accuracy of this approach for materials exhibiting a first-order phase transition has been questioned in the past due to two main issues: the non-homogeneity of samples due to phase coexistence, and the non-equilibrium states exhibited by materials with metastability [39].

Indeed, $\text{Gd}_5\text{Si}_2\text{Ge}_2$ displays both of these phenomena. In this work, we used the following approaches that have been found to successfully mitigate the errors produced by these phenomena:

- measured a small sample (6.93 mg), to facilitate thermal equilibrium with the instrument;
- performed isofield measurements under cooling with a slow temperature sweep rate of 2 K/min, instead of isothermal measurements;
- raised the temperature well above T_C (350 K) between each measurement;
- used a small temperature step to avoid “smearing” the ΔS_M curve and small field step to avoid introducing artificial oscillations from lack of points;
- corrected for demagnetization by measuring an isothermal magnetization at a temperature well below T_C (50 K).

The necessity and validity of these approaches has been discussed in detail in previous works [39, 40, 41, 42].

While we use isofield measurements for the analysis, we also acquired two datasets of magnetization in isothermal conditions (increasing field followed by decreasing field), which help demonstrate the concepts detailed in this section. The isotherms were measured with a magnetic field change rate gradually increasing from 0.5 mT/s (low fields) to 3.5 mT/s (high fields). At every temperature, each pair of isothermal measurements is preceded by a thermal reset in which the sample temperature is increased to 350 K.

2.5. Magnetostatic simulations

The demagnetizing field for samples of highly symmetric shapes, such as rectangular prisms, may be computed analytically by assuming homogeneous magnetization [43]. However, the demagnetizing field and the magnetization, which are interdependent, are often non-homogeneous. Furthermore, an analytical approach is unfeasible for most sample shapes or assemblies of several magnetic bodies. This makes the numerical computation of the demagnetizing field the best approach for accurate determination of the demagnetizing field. This has been previously achieved for assemblies of rectangular prisms by discretizing the shapes into a high number of homogeneously magnetized rectangular cells, combined with the analytical result for homogeneously magnetized rectangular volumes [44, 45]. More recently, the open access tool *FEMCE* employed a finite element method to solve the Maxwell magnetostatic equations for arbitrary shapes [36].

In this study, we use *FEMCE* to obtain the 3D magnetic field distribution within the sample shape at each temperature, applied magnetic intensity, and orientation. To perform these simulations, the workflow was the following: 1) measure magnetization vs. temperature and magnetic field as detailed in the previous section; 2) correct the data for demagnetization, removing existing geometric effects from the dataset (to this end, a magnetization isotherm measured at 50 K was used); 3) export the magnetization data in matrix format, as well as the corresponding temperatures and magnetic fields, to import in *FEMCE*; 4) import the 3D CAD design of the sample shape; 5) create the finite elements mesh for of simulation volume; 6) choose the temperature, applied magnetic field intensity, and orientation. To perform the simulations in sets, we use a version of *FEMCE* without GUI.

3. Results and discussion

We start with the discussion of the direct measurements of the more familiar conventional MCE, followed by the direct measurements of RMCE. We follow the same logic for the indirect measurements (magnetic entropy change), ending with a discussion of the RMCE exhibited for a higher aspect ratio sample.

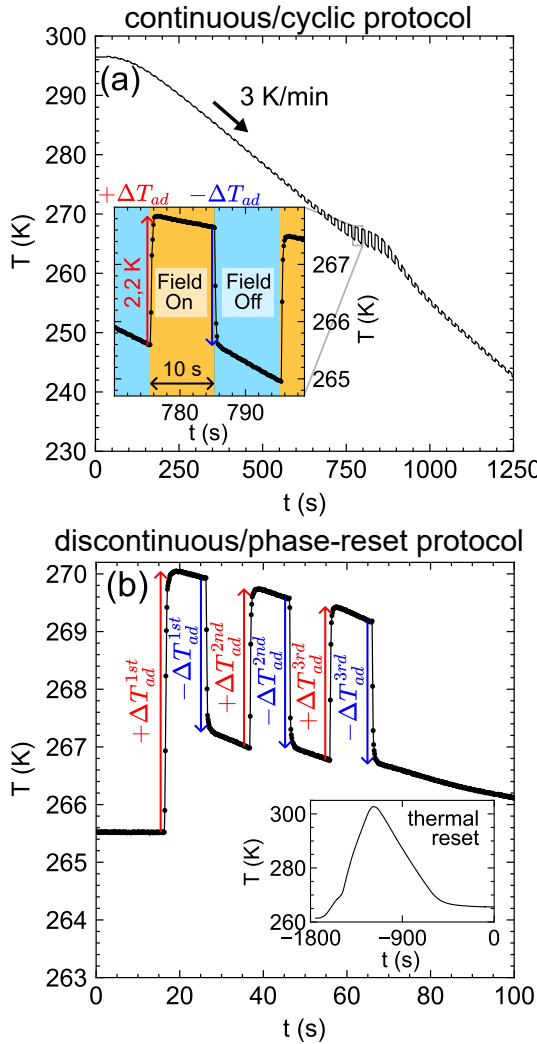


Figure 2: The two direct temperature measurement protocols. (a) Continuous/cyclic protocol under cooling, in which the heat bath temperature of the sample is continuously changing and the field is applied and removed every 10 seconds. (b) The discontinuous/phase-reset protocol, in which the heat bath temperature of the sample is stabilized prior to the field being applied and removed (also every 10 seconds). The discontinuous protocol measurements are always preceded by a thermal reset taking around 30 minutes, as shown in the inset.

3.1. Direct temperature measurements of the conventional magnetocaloric effect

Measurements of ΔT_{ad} at different temperatures in samples without hysteresis can be done by cycling the magnetic field while slowly ramping the heat bath temperature (heating or cooling). This has been referred to as a continuous [46, 47], or cyclic protocol [48]. Within this protocol, we have alternated the magnetic field every 10 seconds, which is exemplified in figure 2. For samples with significant thermal hysteresis, each set of measurements is preceded by a thermal reset, where the sample is heated well above the phase transition temperature, as also done in the magnetization measurements. In this case, the ΔT_{ad} obtained after the first magnetic field application ($+\Delta T_{ad}^{1st}$) will be clearly different from what is obtained after subsequent applications ($+\Delta T_{ad}^{2nd}$ and $+\Delta T_{ad}^{3rd}$), as shown in figure 2(b). This is referred to as the discontinuous [46, 47], or phase-reset [48] protocol.

In figure 3, we show the adiabatic temperature change of the conventional MCE (field application) in (a) a low demagnetizing field orientation (parallel to the sample's larger axis, x, labelled $H_{app} \parallel x$), (b) a high demagnetizing field orientation (parallel to the sample's shortest axis, y, labelled $H_{app} \parallel y$), and (c) the RMCE obtained by

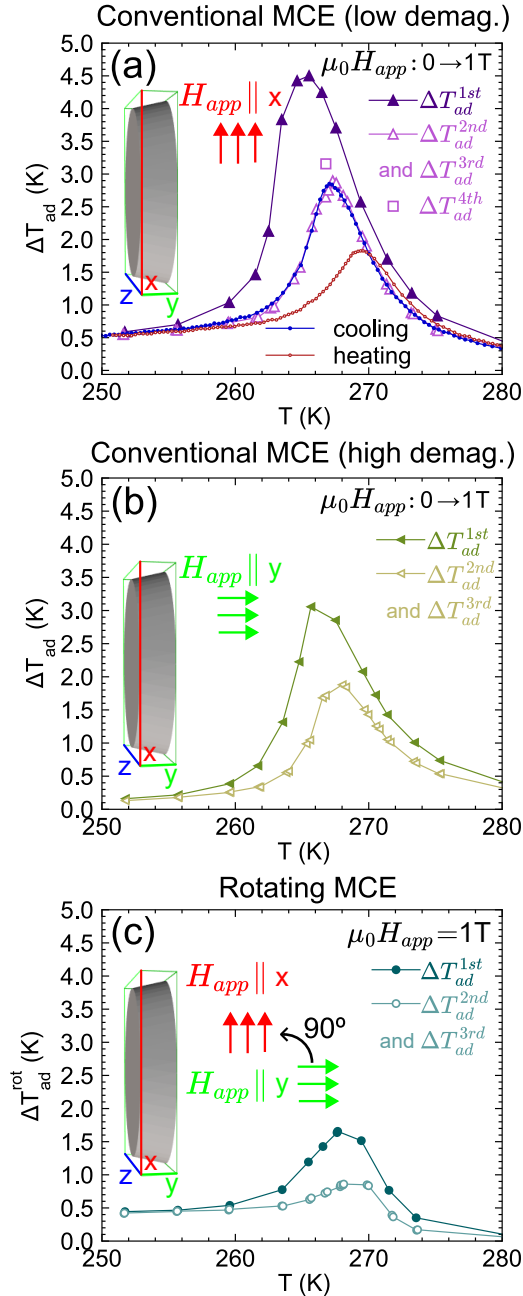


Figure 3: The directly measured ΔT_{ad} values obtained for (a) the low demagnetizing field orientation ($H_{app} \parallel y$) in different measurement protocols, and (b) the high demagnetizing field orientation ($H_{app} \parallel x$). (c) The ΔT_{ad}^{rot} obtained by changing the magnetic field orientation from $H_{app} \parallel x$ to $H_{app} \parallel y$. The "cooling" and "heating" curves in (a) refer to the continuous protocol.

rotating the magnetic field from the high demagnetizing field orientation to the low demagnetizing field orientation ($H_{app} \parallel y \rightarrow H_{app} \parallel x$).

We obtained a remarkable value of maximum $+\Delta T_{ad} = 4.50$ K when applying a 1.0 T magnetic field in the low demagnetizing field orientation at 265.5 K. This is a noteworthy value, because few studies ever directly obtained $|\Delta T_{ad}|$ values above 4 K for such a low magnetic field [3]. Two notable exceptions are $\text{Fe}_{49}\text{Rh}_{51}$, with -4.58 K,

and $\text{Ni}_{45.7}\text{Mn}_{36.6}\text{In}_{13.5}\text{Co}_{4.2}$, with -4.35 K, both with inverse MCE measured for 1.0 T magnetic field applications following discontinuous protocols [47, 49]. Regarding previous studies of $\text{Gd}_5\text{Si}_2\text{Ge}_2$, we are not aware of direct measurements of ΔT_{ad} for a 1.0 T magnetic field. Zeng et al. directly measured a maximum $\Delta T_{ad}=3.9$ K in $\text{Gd}_5\text{Si}_2\text{Ge}_2$ for a 1.5 T magnetic field, but they do not specify the measurement protocol or shape of the sample (which dictates the demagnetizing effect), making comparison difficult [50].

Figure 3(a) also shows the $+\Delta T_{ad}$ values obtained in the second and third magnetic field applications, as well as the values obtained in the continuous protocol (labelled “cooling” and “heating”) with the background temperature being changed at 1 K/min. The reversible ΔT_{ad} obtained in the 2nd and 3rd subsequent field applications is still very significant, reaching a maximum value of 3.16 K at a slightly higher temperature of 266.8 K. This underscores that $\text{Gd}_5\text{Si}_2\text{Ge}_2$ is one of the best magnetocaloric materials with highest ΔT_{ad} at 1.0 T even when considering cyclic conditions, as few materials cross the 3 K threshold [51].

The values of $+\Delta T_{ad}^{2nd}$ and $+\Delta T_{ad}^{3rd}$ measured in the discontinuous protocol have a remarkable agreement with those measured in the continuous protocol during cooling. Thus, the background temperature is varying slowly enough in the continuous protocol (1 K/min) to ensure nearly identical thermodynamic conditions as in the discontinuous protocol (the field applications are also done after cooling in the thermal reset). On the other hand, the curve obtained from the field applications during heating is clearly different: lower in amplitude and shifted to higher temperatures. This difference can be interpreted by the fact that during heating, a field application works against the temperature change in terms of direction of the phase transformation, hindering the MCE more significantly than during cooling, whereas the field applications force the phase transformation to proceed in the same direction as the background temperature change, achieving a partial thermal reset between each field change. Finally, we call attention to a measurement performed at a single temperature, in which the magnetic field is applied a fourth time (labelled ΔT_{ad}^{4th}) within the discontinuous protocol after waiting for the temperature to fully reach the initial one. While ΔT_{ad}^{4th} is still clearly lower than ΔT_{ad}^{1st} , it is a clear outlier from the $+\Delta T_{ad}^{2nd}$ and $+\Delta T_{ad}^{3rd}$ curve, implying that there is a range of values that the $+\Delta T_{ad}$ of subsequent field applications can take, depending on how long one waits for the sample temperature to return to the initial value.

The maximum $+\Delta T_{ad}$ obtained when applying a 1.0 T field in the high demagnetizing field orientation was 3.06 K, at 265.7 K. While still very significant, it is only 68% of the maximum value obtained when the field was applied in the low demagnetizing field orientation. This highlights the importance of either minimizing or taking demagnetization into account when measuring the MCE. At the same time, the 32% difference between the peak $+\Delta T_{ad}$ obtained for the different orientations already suggests the potential of achieving a high $+\Delta T_{ad}^{rot}$ exclusively through a change in the demagnetizing field. Indeed, in a material without hysteresis and other sources of anisotropy, it is expected that the demagnetizing field-based rotating MCE is approximately equal to the difference of the conventional MCE exhibited in each orientation [28].

3.2. Direct temperature measurements of the rotating magnetocaloric effect

During the thermal reset performed for the RMCE measurements, the magnetic field remains applied along the high demagnetizing field orientation until the measurement temperature stabilizes. Then, the field is rotated every 10 s as in the discontinuous protocol, similarly to the measurements of the conventional MCE shown in figure 2(b).

Figure 3(c) shows the ΔT_{ad}^{rot} (RMCE) obtained in the discontinuous protocol when rotating the applied magnetic field from the high demagnetizing field orientation to the low demagnetizing field orientation. The peak value of ΔT_{ad}^{rot} measured for 1.0 T was 1.66 K at 267.7 K, 37% of the maximum value obtained for the conventional MCE in the low demagnetizing field orientation. Notably, the peak value of the RMCE closely corresponds to the difference of the conventional MCE amplitudes for the different field orientations (1.44 K).

Some insight into the shape of the $\Delta T_{ad}^{rot}(T)$ curve seen in figure 3(c) can also be given by examining the two $\Delta T_{ad}(T)$ curves shown in figures 3(a) and (b): the starker difference between these two curves occurs below the phase transition temperature at 1.0 T, around 270 K, since the magnetization increases drastically, in turn making the demagnetizing effect more significant. Consequently, the temperature profile of $\Delta T_{ad}^{rot}(T)$ is asymmetrical, having a higher tail towards low temperatures, where the internal magnetic field change between the two orientations is larger. This effect will be examined and explained through the magnetostatic simulations shown further ahead.

Figure 4 shows the ΔT_{ad}^{rot} obtained through the discontinuous protocol for different applied magnetic field amplitudes. Considering the peak amplitudes obtained at different field intensities, a non-monotonous behaviour is observed, in which the peak amplitude very quickly increases, until 0.8 T, where it reaches its peak, and then decreases for the 1.0 T field amplitude. Simultaneously, the 0.8 T and 1.0 T curves show a slight shift to higher temperatures,

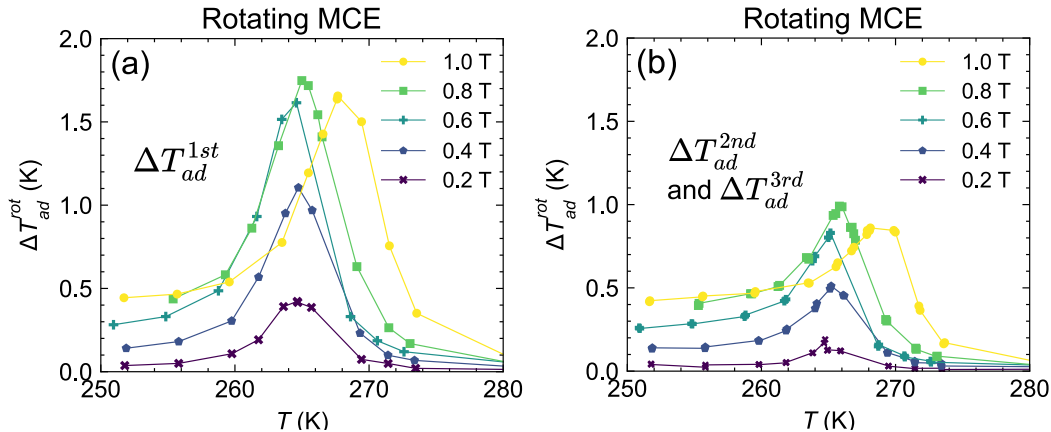


Figure 4: The directly measured ΔT_{ad}^{rot} obtained through the discontinuous protocol for the rotation of different applied magnetic field intensities on the (a) first magnetic field application (irreversible), and (b) subsequent magnetic field rotations. All values correspond to rotation from high to low demagnetizing field orientations, as illustrated in figure 3.

which is distinct behavior than previously observed for the RMCE in Gd [28]. On the other hand, the non-monotonous behavior is quite comparable to what was found in Gd.

The highest ΔT_{ad}^{rot} measured overall was 1.77 K, obtained for the first 0.8 T field rotation at 265 K (figure 4(a)). It is interesting to note that RMCE under the applied field as low as 0.6 T is already comparable to the RMCE obtained for the 1 T field. This emphasizes that any future prototype utilizing RMCE should aim at using low magnetic fields, as previously suggested [28]. Figure 4 (b) shows the ΔT_{ad}^{rot} values obtained for subsequent magnetic field rotations, which are all similarly attenuated due to the metastability of the sample, as shown for the measurements obtained in 1 T shown in figure 3.

Furthermore, to our knowledge, this is the highest ΔT_{ad}^{rot} ever measured under a constant external magnetic field in a material without any MCA. Even for those with MCA, few materials reach values above 2 K for low fields, with some prominent examples being NdCo_5 for 2 T or $\text{NdCo}_{4.2}\text{Fe}_{0.8}$ for 1 T or 2 T [52]. Such values may be achievable in $\text{Gd}_5\text{Si}_2\text{Ge}_2$ exclusively through the demagnetizing effect by shaping the sample in a shape with a higher aspect ratio, as suggested by the results of simulations shown in the following sections.

3.3. Indirect measurements of the conventional magnetocaloric effect - magnetic entropy change during field application

Figure 5 shows magnetization data sets acquired using different protocols mentioned in section 2. Isothermal curves plotted from the isofield measurements performed as a function of temperature (figure 5(d)) highly resemble the values acquired through isothermal measurements in decreasing field (figure 5(b)). Contrastingly, the magnetization obtained in isothermal measurements with increasing field (figure 5(a)) displays evidence of significant phase coexistence, even though the phase transformation direction is the same as during decreasing temperature. This makes the increasing field dataset prone to artificial peaks of ΔS_M , as discussed in [39, 40]. The chosen dataset for our study were the isofield curves obtained under cooling shown in figure 5(c) and figure 5(d), as they more closely correspond to the thermodynamic path followed in the stable protocol of the direct temperature measurements, as these were also preceded by a thermal reset.

To determine ΔS_M taking demagnetization into account, we must first compute what the internal field is for each applied magnetic field intensity. This is where the magnetostatic simulations become necessary. These simulations allow us to estimate the internal magnetic field as a function of temperature and applied (external) field amplitude at each point of the sample's volume. In each computation, constant temperature throughout the sample is assumed. As such, the finite elements of the sample have the same $\mathbf{M}(\mathbf{H})$ response, corresponding to the isothermal magnetization at the simulation temperature. However, the converged solution of the system allows for a different internal magnetic field at each element.

Figure 6 shows the results of a pair of simulations done for 260 K and an applied field of 1.0 T applied for the high demagnetizing field ($H_{app} \parallel y$) and low demagnetizing field ($H_{app} \parallel x$) orientations. The sample was discretized into

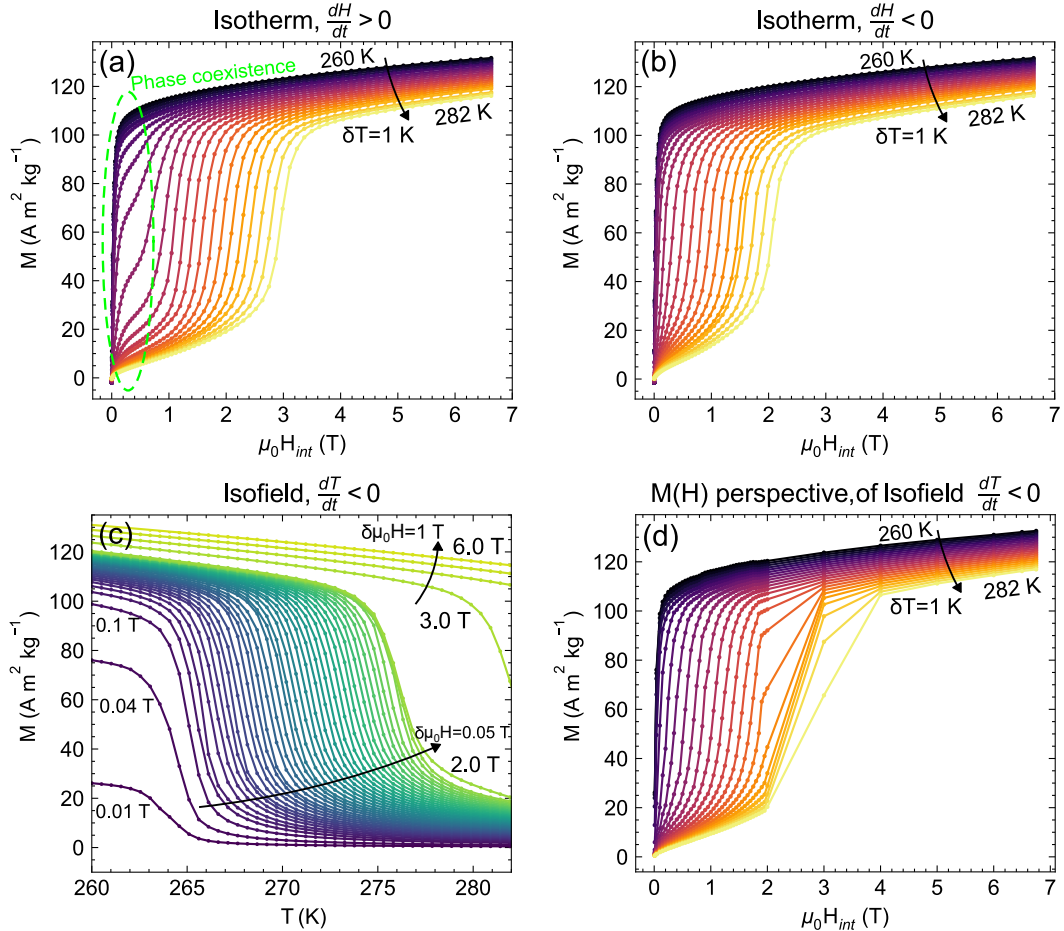


Figure 5: The different magnetization datasets acquired through different protocols. Magnetization isotherms measured with (a) increasing magnetic field and (b) decreasing magnetic field. Magnetization isofield curves measured under cooling with a constant applied magnetic field are plotted (c) versus temperature and (d) versus magnetic field, to facilitate comparison with the curves measured with constant temperature. The sample temperature is raised to 350 K between each pair of isotherms and each isofield measurement.

41594 elements. The statistical distribution of internal fields for each orientation is shown in the histograms in figure 6(a) and 6(d). In this low temperature example, when the magnetization is the highest, the differences in the internal field distributions are very significant, with the high demagnetizing field orientation having more variance and a tail towards high fields, and the orientation for low demagnetizing field having a tail towards lower fields.

The volume-average of the internal field intensities (marked as the dashed vertical line) is 0.34 T and 0.85 T for the high demagnetizing field and low demagnetizing field orientations, respectively. Figures 6(b) and 6(e) are 3D scatter plots, in which each sphere represents the centroid of an element and its colour the internal field intensity at that element. Since the 3D plot only allows us to see the outer layer of the elements, in the figures 6(c) and 6(f) the volume-average internal field magnitude across the entire thickness of the sample is plotted in 2D.

These computations also allow the determination of an effective demagnetizing factor, D_{eff} . Since we have access to the magnetization and internal fields in each element, we can relate the average internal field and the applied fields through:

$$\langle H_{int} \rangle = H_{app} - D_{eff} \langle M(H_{int}) \rangle, \quad (2)$$

where rearranging yields the explicit expression:

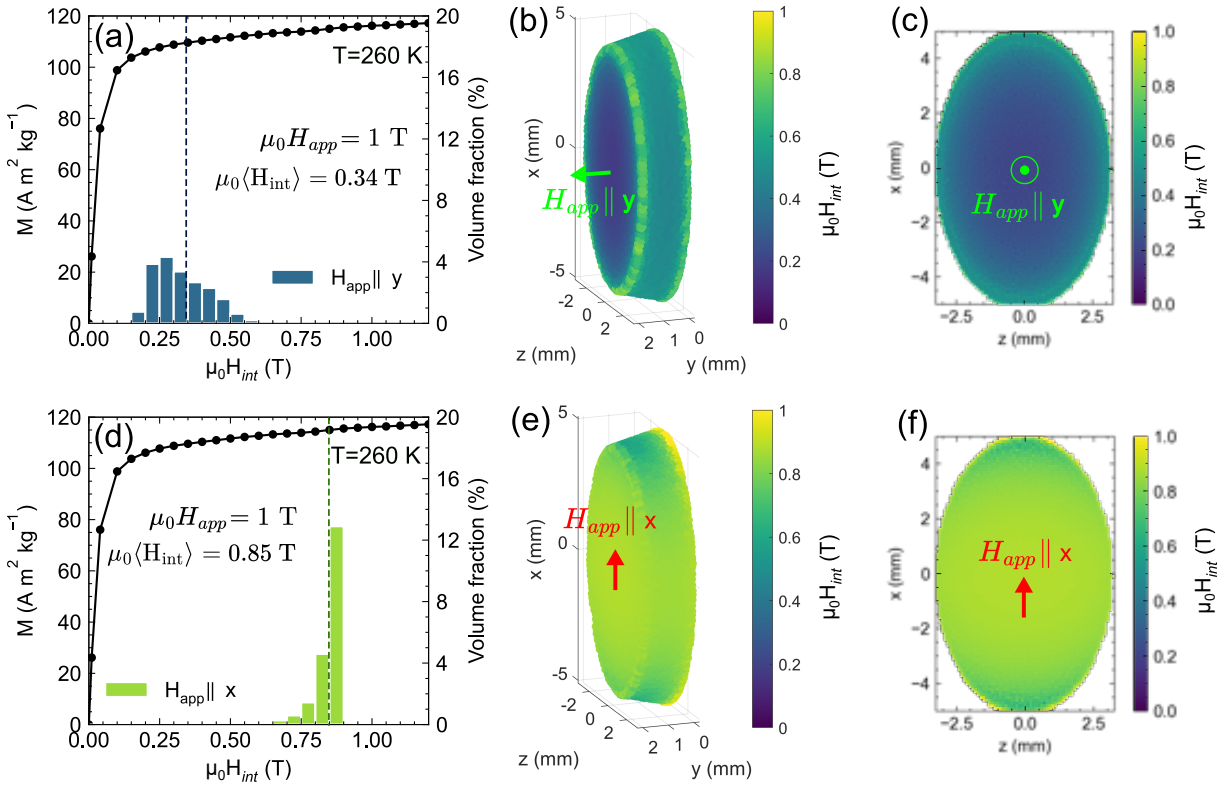


Figure 6: FEMCE magnetostatic simulations for two magnetic field orientations at 260 K. The magnetization isotherm for the simulation temperature, shown together with the histogram of the internal magnetic field intensities for the (a) high demagnetizing field orientation and (d) the low demagnetizing field orientation. The results of the simulation in a 3D scatter plot for the (b) high and (e) low demagnetizing field orientations. The volume-average of the field intensities over the thickness of the sample is shown in 2D for the (c) high and (f) low demagnetizing field orientations.

$$D_{eff} = \frac{H_{app} - \langle H_{int} \rangle}{\langle M(H_{int}) \rangle}. \quad (3)$$

In these expressions, the *volumetric* magnetization should be considered, which was obtained by considering the density of $\text{Gd}_5\text{Si}_2\text{Ge}_2$ from the literature, 7.521 g/cm³ [53].

Applying this procedure for the case shown in figure 6, we obtain $D_{eff}^{\parallel} = 0.13$ and $D_{eff}^{\perp} = 0.62$ for the low demagnetizing field and high demagnetizing field orientations, respectively. These figures vary slightly with temperature and applied field intensity. D_{eff}^{\parallel} varies between 0.127 and 0.140, and D_{eff}^{\perp} varies between 0.566 and 0.653. The value of D_{eff} does not convey any information about the shape of the distribution of internal field intensity, but it is useful to quantify the intensity of demagnetization and allow comparisons between different shapes.

These simulations were computed in 0.5 K steps from 260 K to 280 K and 0.2 T steps from 0.2 T to 2.0 T for each applied field orientation, corresponding to a total of 810 computations and allowing us to use equation 1 to compute the ΔS_M^{rot} between the average internal fields at each configuration (referred in shorthand simply as H1 for the high demagnetizing field orientation and H2 for the low demagnetizing field orientation, which are functions of temperature and applied field amplitude). There was no discernible difference found between computing the average ΔS_M for the internal field variation of each element or computing ΔS_M for the overall change in average internal field, so we will proceed with the more intuitive approach of computing the integral between the two average field intensities.

The simulation results are shown in figure 7. Figure 7(a) and 7(b) show the obtained average internal fields for each applied magnetic field orientation. Figure 7(c) shows the difference between the corresponding average internal fields. For every applied field intensity, a clear reduction of the internal field occurs on cooling at the phase transition

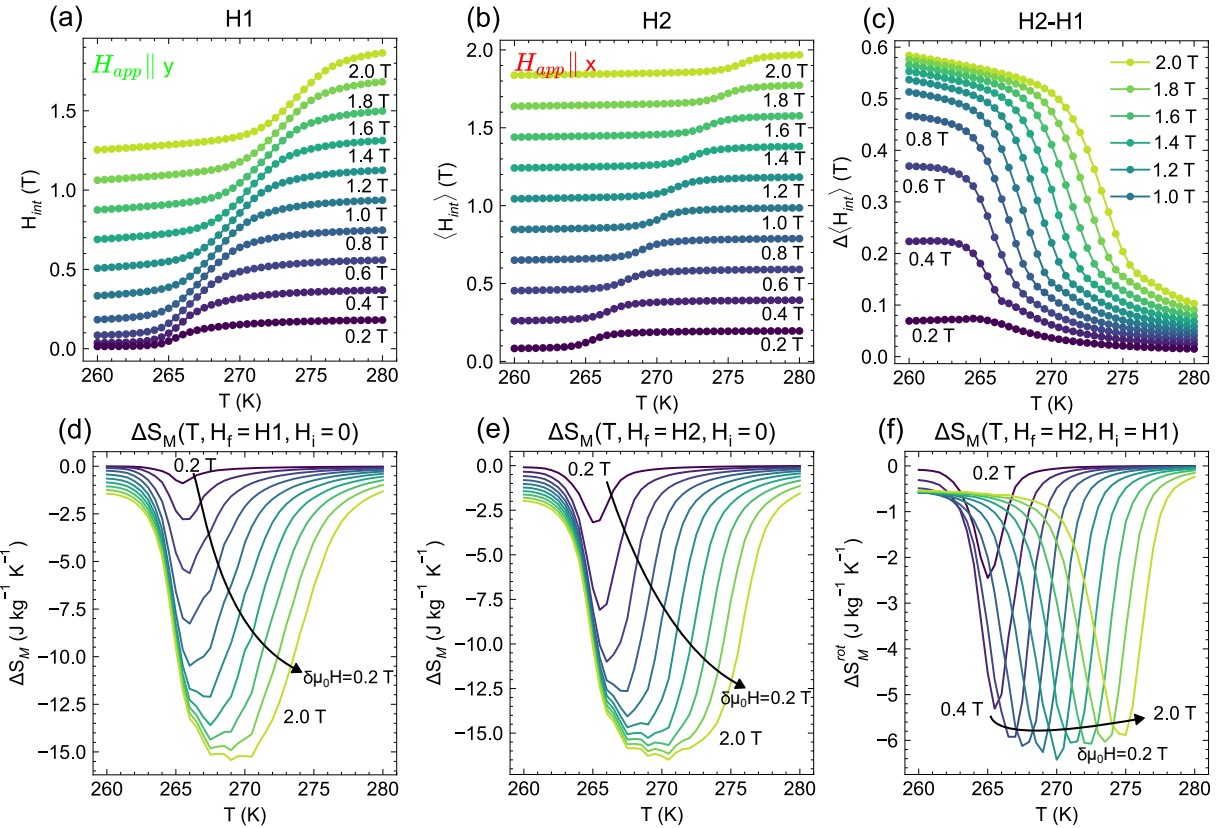


Figure 7: The average internal magnetic field intensities obtained from the *FEMCE* simulations for every temperature and external magnetic field intensity for the (a) high demagnetizing field orientation, (b) low demagnetizing field orientation, and (c) the difference between the two. In the lower part, we see the obtained ΔS_M for the magnetic field applications along the (d) high demagnetizing field orientation, (e) low demagnetizing field orientation, and (f) the difference between the two, corresponding to ΔS_M^{rot} .

temperature, which shifts towards higher temperatures with increasing field intensity. Figures 7(d) and 7(e) and correspond to the ΔS_M of the conventional MCE, which was obtained by computing equation 1 for an initial internal field (H_i) intensity of 0 and a final internal field intensity (H_f) equal to the corresponding average internal field (H1 or H2, respectively).

The maximum ΔS_M obtained for the low demagnetizing field orientation was $-16.49 \text{ J K}^{-1} \text{ kg}^{-1}$, in good agreement with a previous study following similar measurement procedures ($-18.73 \text{ J K}^{-1} \text{ kg}^{-1}$ after correcting for the demagnetizing field) [42].

3.4. Indirect measurements of the rotating magnetocaloric effect - magnetic entropy change during field rotation

The maximum ΔS_M obtained for the high demagnetizing field orientation was $-15.43 \text{ J K}^{-1} \text{ kg}^{-1}$, corresponding to a reduction of only 6% with respect to the low demagnetizing field orientation. This could lead one to assume that changing D_{eff} from ~ 0.6 to ~ 0.1 in fact had a very small impact, leading to a small RMCE. However, one may notice from figures 7(d) and (e) that the widths of the ΔS_M curves for the two orientations are quite different, in particular at the temperatures above the phase transition. Since the ΔS_M has a very sharp dependence for lower fields near the phase transition temperature, a change of demagnetizing factor has a small effect on ΔS_M in that region. At the same time, increasing the applied field intensity leads to a slightly increased peak but also a widening of the ΔS_M profile towards higher temperatures, which is a typical characteristic of magnetocaloric materials with FOPT [9]. The impact of the demagnetizing effect is mostly translated through a diminished widening with increased field amplitudes. This

contrasts with what has been previously found for Gd [28]. The temperature profile of the SOPT of Gd is such that increasing the field raises ΔS_M in general, instead of a clearly asymmetrical increase.

The entropy change resulting from rotation, ΔS_M^{rot} , corresponds precisely to the difference between the ΔS_M obtained for each applied magnetic field orientation (which results directly from the fundamental theorem of calculus applied to equation 1). This is shown in figure 7(f). Even though the change in average internal field intensity (H2-H1) increases monotonously with applied field intensity, as shown in figure 7(c), ΔS_M^{rot} has an extremely non-monotonous field-dependence, in which saturation is very quickly reached while a shift to higher temperature occurs. For instance, the maximum ΔS_M^{rot} obtained for 0.8 T, $-6.12 \text{ J K}^{-1} \text{ kg}^{-1}$, corresponds to 95% of the global maximum ΔS_M^{rot} reached, which was $-6.42 \text{ J K}^{-1} \text{ kg}^{-1}$ at 1.2 T. These amplitudes of the peak entropy change obtained for the RMCE without changing the applied field intensity (only rotating its orientation) are noteworthy, surpassing the peak values obtained by several other prominent magnetocaloric materials through the conventional MCE even for higher applied field intensities [54]. This further implies that from the perspective of RMCE application, the use of high magnetic fields (>1 T) is unnecessary and, likely, wasteful.

3.5. Improving the rotating magnetocaloric effect by increasing the aspect ratio and comparison with SOPT gadolinium

Using a real sample with a large aspect ratio, we already demonstrated significant RMCE values in $\text{Gd}_5\text{Si}_2\text{Ge}_2$ material. However, as explained in section 2, the RMCE could be further improved in a sample with a more extreme aspect ratio. To explore this possibility, we performed simulations of a thin rectangular prism with an aspect ratio of 20 (20 mm by 20 mm by 1 mm) and compared it to the results of the experimentally measured shape. Furthermore, we perform simulations for a Gd sample with the same thin plate shape, to compare the RMCE of the two materials for the same shape. The results are shown in figure 8.

Changing the shape from the experimentally measured one to the simulated thin plate decreased D_{eff}^{\parallel} from 0.13 to 0.05 and increased D_{eff}^{\perp} from 0.62 to 0.85. Figure 8(a) shows the conventional MCE for the low demagnetizing field orientation of the thin plate ("in plane"), the high demagnetizing field orientation ("off plane"), and the RMCE obtained from a rotation between the two. The magnetic entropy change for the thin plate of Gd reached $-8.67 \text{ J K}^{-1} \text{ kg}^{-1}$, which is 35% more than the maximum obtained for the experimentally measured shape. The difference between the ΔS_M temperature profiles of the RMCE curves obtained for $\text{Gd}_5\text{Si}_2\text{Ge}_2$ and Gd's SOPT is also very clear, as described above.

The non-monotonous field-dependence of the RMCE obtained for both materials and shapes is shown in figure 8(b). The peak RMCE of $\text{Gd}_5\text{Si}_2\text{Ge}_2$ is over 5 times bigger than that obtained from the simulations for Gd for both shapes. It is clear from this astounding difference that FOPT materials have more potential to achieve high RMCE due to their sharp (in temperature) phase transition, as well as the significant shift of the phase transition temperature with magnetic field.

Finally, it is worth highlighting that the intensity of the magnetic entropy change is inextricably linked to its "width" (in temperature). It is often the case that the high peaks of ΔS_M displayed by materials with GMCE come at the cost of slimmer profiles in temperature, and the same has been found for the RMCE. The temperature-averaged entropy change (TEC), previously proposed by L. D. Griffith et al. [55], is a figure of merit that better conveys the temperature profile of ΔS_M . It is defined as

$$TEC(\Delta T_{lift}) = \frac{\max \left\{ \int_{T_{mid} - \frac{\Delta T_{lift}}{2}}^{T_{mid} + \frac{\Delta T_{lift}}{2}} \Delta S_M(T) dT \right\}}{\Delta T_{lift}}, \quad (4)$$

where T_{lift} is the temperature lift over which the average is evaluated and T_{mid} is the middle temperature which maximizes the average for the chosen temperature lift.

The field-dependence of the TEC for a temperature lift of 10 K can be seen in figure 8(c) for both sample shapes. For the chosen temperature lift, $\text{Gd}_5\text{Si}_2\text{Ge}_2$ still clearly outperforms Gd, however, the wider temperature profile of Gd's ΔS_M reduces the improvement margin from over 5 times larger to between 2 and 3 times larger for either shape.

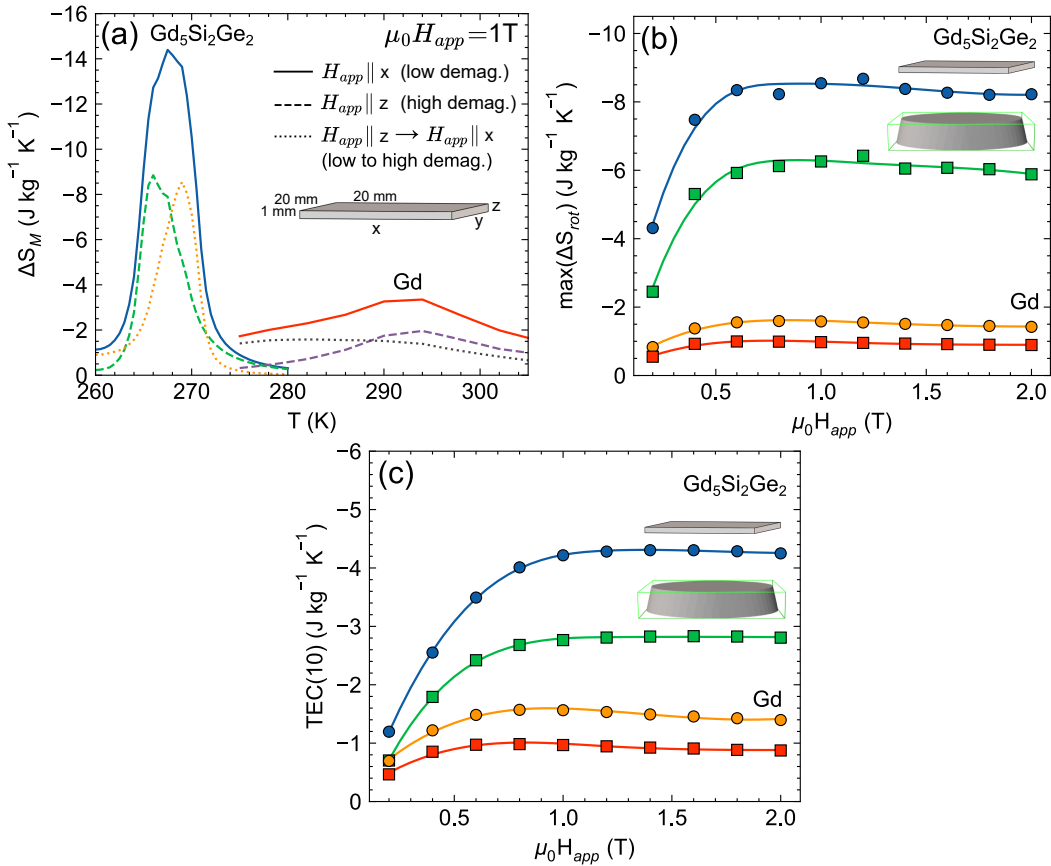


Figure 8: (a) The isothermal entropy change of the conventional (continuous line for low demagnetizing field orientation and dashed line for high demagnetizing field orientation) and rotating (dotted line) MCE of $\text{Gd}_5\text{Si}_2\text{Ge}_2$ and Gd for a thin plate sample shape with aspect ratio of 20. (b) and (c) show the peak ΔS_M^{rot} and TEC(10) values as a function of applied magnetic field amplitude for both materials with the thin plate shape (circles) and the experimentally measured shape (squares).

4. Conclusions and outlook

We have extensively characterized the demagnetizing field-based rotating magnetocaloric effect of a first-order magnetocaloric material, $\text{Gd}_5\text{Si}_2\text{Ge}_2$, for the first time via two complementary approaches.

Both the ΔT_{ad}^{rot} and ΔS_M^{rot} were found to very quickly increase with the applied magnetic field amplitude and then decrease, while shifting toward higher temperatures. The maximum ΔT_{ad}^{rot} obtained was 1.77 K for 0.8 T, and the maximum ΔS_M^{rot} was $-6.42 \text{ J K}^{-1} \text{ kg}^{-1}$, for 1.2 T. For 0.8 T, ΔS_M^{rot} already reaches $-6.12 \text{ J K}^{-1} \text{ kg}^{-1}$, 95 % of its maximum value, higher than the maximum ΔS_M obtainable in the conventional MCE of Gd with 1.0 T. Our study suggests that the RMCE is fundamentally suited for low magnetic field applications, particularly in first-order magnetocaloric materials.

Finally, the already impressive peak ΔS_M^{rot} of the experimentally measured shape was found to increase by 35% in a sample with a more extreme aspect ratio of 20. A proportional increase of the maximum ΔT_{ad}^{rot} would raise it over 2 K, which recently has been suggested as an important threshold required for developing efficient refrigeration devices [5], reinstating the demagnetizing field-based RMCE's relevance in magnetic refrigeration, in particular for magnetocaloric materials with FOPT. While the non-monotonous field-dependence of the RMCE had been previously found for Gd, the overall temperature-dependence of the RMCE in $\text{Gd}_5\text{Si}_2\text{Ge}_2$ was fundamentally different due to its first-order phase transition, which is much sharper in temperature for all magnetic fields measured and significantly shifts towards high temperatures with increasing applied field.

The results of our work clearly show the significant influence of the material's shape both for the conventional and rotating MCE, hopefully informing future studies of GMCE materials.

Regarding heat pumping applications, we underline that, while the RMCE enables a different kind of device design, where no field intensity modulation is needed, potentially reducing the total volume of permanent magnets required, some new challenges are also expected. Namely, if the magnetic field region used in the device is cylindrical, packing as much magnetocaloric material as possible within it (porosities are usually below 50% [2]) will inevitably lead to an overall reduction of the aspect ratio, thus decreasing the RMCE in comparison with what is possible with an isolated, high aspect ratio plate [45]. This leads to a complex optimization problem, where increasing material content simultaneously decreases the intensity of the effect, while also altering the thermofluidic properties. This investigation will be detailed in future works.

Acknowledgements

The authors acknowledge FCT and its support through the projects LA/P/0095/2020, UIDB/04968/2025, and UIDP/04968/2025. R. Almeida thanks FCT for his PhD grant with reference 2022.13354.BD and DOI <https://doi.org/10.54499/2022.13354.BD>. This project has received funding from the European Union's Horizon Europe research and innovation programme through the European Innovation Council under the grant agreement No. 101161135 – MAGCCINE. This work was also developed within the scope of the project CICECO-Aveiro Institute of Materials, UIDB/50011/2020, UIDP/50011/2020 & LA/P/0006/2020, financed by national funds through the FCT/MCTES (PIDDAC). The work at the Ames National Laboratory (Y.M. and K. D.-A.) on material's synthesis and manuscript editing was supported by the Division of Materials Science and Engineering of the Office of Basic Energy Sciences, Office of Science of the U.S. Department of Energy (DOE). Ames National Laboratory is operated for the U.S. DOE by Iowa State University of Science and Technology under Contract No. DE-AC02-07CH11358.

A. Magnetic and structural characterization

The main phase of $\text{Gd}_5\text{Si}_2\text{Ge}_2$ exhibits the first-order magnetostructural phase transition behind its GMCE near 270 K. From low to high temperature, it transforms from an orthorhombic-II ferromagnetic phase to a monoclinic paramagnetic phase [17]. At higher temperatures, a small fraction of $\text{Gd}_5\text{Si}_2\text{Ge}_2$ phase remains orthorhombic and ferromagnetic, exhibiting a second-order phase transition to a paramagnetic state near 300 K. Our findings, shown in figure 9, are consistent with the literature.

Another sample was extracted from the same batch as the other samples used in this study and measured in powder X-ray diffraction at room temperature. The Rietveld refinement results are shown in figure 10. The pattern show a clear match (GOF = 1.3) with the reported monoclinic $\text{Gd}_5\text{Si}_2\text{Ge}_2$ crystal structure with lattice parameters: $a = 0.75788$ nm, $b = 1.48011$ nm, $c = 0.77804$ nm, and $\gamma = 93.17$ deg [35].

CRediT authorship contribution statement

Rafael Almeida: Conceptualization, Software, Formal analysis, Investigation, Data Curation, Writing – Original Draft, Writing – Review & Editing, Visualization. **Rodrigo Kiefe:** Methodology, Software, Validation, Writing – Review & Editing. **Ricardo Moura Costa Pinto:** Investigation, Writing – Review & Editing. **João Sequeira Amaral:** Conceptualization, Investigation, Writing – Review & Editing, Funding Acquisition. **Kyle Dixon-Anderson:** Investigation, Formal analysis, Resources, Writing – Review & Editing. **Yaroslav Mudryk:** Resources, Writing – Review & Editing, Supervision, Funding acquisition. **João Pedro Araújo:** Writing – Review & Editing, Supervision, Funding acquisition. **João Horta Belo:** Conceptualization, Investigation, Writing – Review & Editing, Supervision, Funding acquisition, Project administration.

References

- [1] A. Tishin and Y. Spichkin, *The Magnetocaloric Effect and its Applications*. CRC Press, 4 2016.
- [2] A. Kitanovski, J. Tušek, U. Tomc, U. Plazník, M. Ožbolt, and A. Poredoš, *Magnetocaloric Energy Conversion*, vol. 179. Springer Cham, 2015.

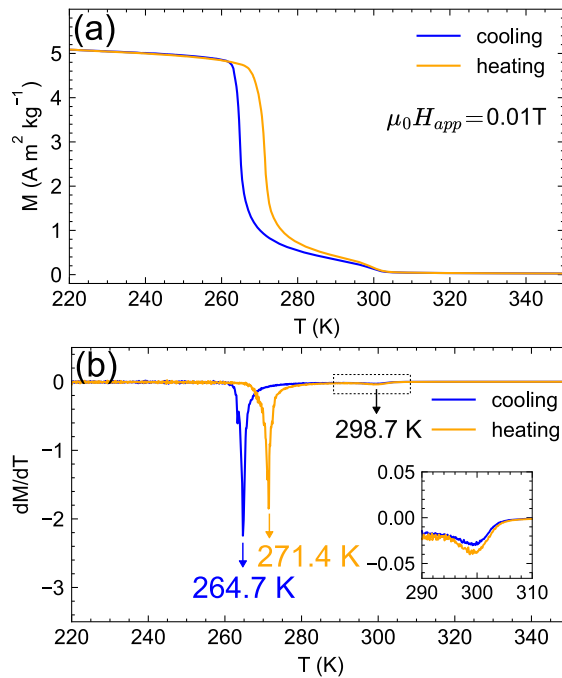


Figure 9: (a) Isofield magnetization on cooling and heating with a 0.01 T applied magnetic field, measured at a temperature change rate of 2 K/min. (b) The derivatives of the two curves, showing peaks at the phase transition temperatures.

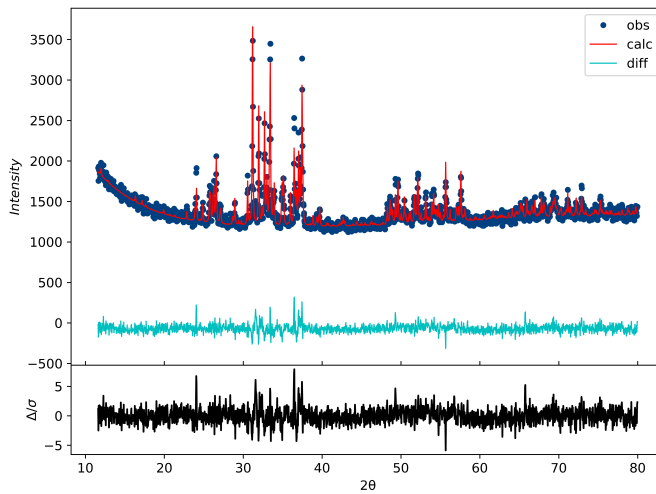


Figure 10: Powder X-ray diffraction measurements of the prepared $\text{Gd}_5\text{Si}_2\text{Ge}_2$ at room temperature and Rietveld refinement results.

- [3] V. Franco, J. S. Blázquez, J. J. Ipus, J. Y. Law, L. M. Moreno-Ramírez, and A. Conde, “Magnetocaloric effect: From materials research to refrigeration devices,” *Pro. Mater. Sci.*, vol. 93, pp. 112–232, 4 2018.
- [4] Y. Hwang and S. Qian, “Caloric Cooling Technologies: 50th Informatory Note on Refrigeration Technologies,” *International Institute of Refrigeration (IIR)*, 2022.
- [5] K. Klinar, J. Y. Law, V. Franco, X. Moya, and A. Kitanovski, “Perspectives and Energy Applications of Magnetocaloric, Pyromagnetic, Electrocaloric, and Pyroelectric Materials,” *Advanced Energy Materials*, vol. 14, no. 39, p. 2401739, 2024.

- [6] W. Thomson, "II. On the thermoelastic, thermomagnetic, and pyroelectric properties of matter," *The London, Edinburgh, and Dublin Philosophical Magazine and Journal of Science*, vol. 5, no. 28, pp. 4–27, 1878.
- [7] A. Smith, "Who discovered the magnetocaloric effect?," *The European Physical Journal H*, vol. 38, pp. 507–517, 06 2013.
- [8] G. V. Brown, "Magnetic heat pumping near room temperature," *Journal of Applied Physics*, vol. 47, pp. 3673–3680, 08 1976.
- [9] A. Smith, C. R. Bahl, R. Bjork, K. Engelbrecht, K. K. Nielsen, and N. Pryds, "Materials challenges for high performance magnetocaloric refrigeration devices," *Adv. Energy Mater.*, vol. 2, pp. 1288–318, 11 2012.
- [10] G. V. Brown and S. S. Papell, "Regeneration tests of a room temperature magnetic refrigerator and heat pump," *arXiv:1402.3343 [physics.ins-det]*, 2014.
- [11] S. Nikitin, G. Myalikgulyev, A. Tishin, M. Annaorazov, K. Asatryan, and A. Tyurin, "The magnetocaloric effect in $\text{Fe}_{49}\text{Rh}_{51}$ compound," *Physics Letters A*, vol. 148, no. 6, pp. 363–366, 1990.
- [12] V. K. Pecharsky and K. A. Gschneidner, "Giant magnetocaloric effect in $\text{Gd}_5(\text{Si}_2\text{Ge}_2)$," *Physical Review Letters*, vol. 78, pp. 4494–4497, 6 1997.
- [13] J. Liu, X. You, B. Huang, I. Batashev, M. Maschek, Y. Gong, X. Miao, F. Xu, N. van Dijk, and E. Brück, "Reversible low-field magnetocaloric effect in Ni-Mn-In-based Heusler alloys," *Phys. Rev. Mater.*, vol. 3, p. 084409, Aug 2019.
- [14] S. Lointe, A. Barcza, M. Risser, C. Muller, and M. Katter, "LaFeSi-based magnetocaloric material analysis: Cyclic endurance and thermal performance results," *International Journal of Refrigeration*, vol. 124, pp. 43–51, 2021.
- [15] J. Lai, X. You, J. Law, V. Franco, B. Huang, D. Bessas, M. Maschek, D. Zeng, N. van Dijk, and E. Brück, "Ultra-low hysteresis in giant magnetocaloric $\text{Mn}_{1-x}\text{V}_x\text{Fe}_{0.95}(\text{P},\text{Si},\text{B})$ compounds," *Journal of Alloys and Compounds*, vol. 930, p. 167336, 2023.
- [16] J. Y. Law, L. M. Moreno-Ramírez, Á. Díaz-García, and V. Franco, "Current perspective in magnetocaloric materials research," *Journal of Applied Physics*, vol. 133, p. 040903, 01 2023.
- [17] Y. Melikhov, R. Hadimani, and A. Raghunathan, "Gd₅(SixGe_{1-x})₄ system – updated phase diagram," *Journal of Magnetism and Magnetic Materials*, vol. 395, pp. 143–146, 2015.
- [18] S. A. Nikitin, K. P. Skokov, Y. S. Koshkid'Ko, Y. G. Pastushenkov, and T. I. Ivanova, "Giant rotating magnetocaloric effect in the region of spin-reorientation transition in the NdCo₅ single crystal," *Physical Review Letters*, vol. 105, p. 137205, 9 2010.
- [19] M. Balli, S. Jandl, P. Fournier, and M. M. Gospodinov, "Anisotropy-enhanced giant reversible rotating magnetocaloric effect in HoMn_2O_5 single crystals," *Applied Physics Letters*, vol. 104, p. 232402, 6 2014.
- [20] H. Zhang, Y. Li, E. Liu, Y. Ke, J. Jin, Y. Long, and B. Shen, "Giant rotating magnetocaloric effect induced by highly texturing in polycrystalline DyNiSi compound," *Scientific Reports 2015 5:1*, vol. 5, pp. 1–10, 7 2015.
- [21] C. R. Bahl and K. K. Nielsen, "The effect of demagnetization on the magnetocaloric properties of gadolinium," *J. Appl. Phys.*, vol. 105, p. 13916, 2009.
- [22] M. D. Kuzmin, K. P. Skokov, D. Y. Karpenkov, J. D. Moore, M. Richter, and O. Gutfleisch, "Magnetic field dependence of the maximum adiabatic temperature change," *Applied Physics Letters*, vol. 99, p. 12501, 7 2011.
- [23] K. K. Nielsen, A. Smith, C. R. Bahl, and U. L. Olsen, "The influence of demagnetizing effects on the performance of active magnetic regenerators," *Journal of Applied Physics*, vol. 112, p. 94905, 11 2012.

[24] P. V. Trevizoli, J. R. Barbosa, P. A. Oliveira, F. C. Canesin, and R. T. Ferreira, “Assessment of demagnetization phenomena in the performance of an active magnetic regenerator,” *International Journal of Refrigeration*, vol. 35, pp. 1043–1054, 6 2012.

[25] C. Romero-Muñiz, J. J. Ipus, J. S. Blázquez, V. Franco, and A. Conde, “Influence of the demagnetizing factor on the magnetocaloric effect: Critical scaling and numerical simulations,” *Applied Physics Letters*, vol. 104, p. 252405, 06 2014.

[26] J. A. Barclay, W. C. Overton Jr., and W. F. Stewart, “MAGNETIC REFRIGERATION APPARATUS AND METHOD,” *United States Patent US4459811A*, 1984.

[27] Q. Badosa, L. Mañosa, E. Vives, A. Planes, B. Weise, L. Beyer, and E. Stern-Taulats, “Demagnetizing field-induced magnetocaloric effect in Gd ,” *J. Appl. Phys.*, vol. 134, 9 2023.

[28] R. Almeida, S. C. Freitas, C. R. Fernandes, R. Kiefe, J. P. Araújo, J. S. Amaral, J. O. Ventura, J. H. Belo, and D. J. Silva, “Rotating magnetocaloric effect in polycrystals—harnessing the demagnetizing effect,” *Journal of Physics: Energy*, vol. 6, p. 015020, 1 2024.

[29] S. L. Russek and C. B. Zimm, “Potential for cost effective magnetocaloric air conditioning systems,” *International Journal of Refrigeration*, vol. 29, no. 8, pp. 1366–1373, 2006. Magnetic Refrigeration at Room Temperature.

[30] A. Tura and A. Rowe, “Permanent magnet magnetic refrigerator design and experimental characterization,” *International Journal of Refrigeration*, vol. 34, no. 3, pp. 628–639, 2011.

[31] R. Bjørk, C. Bahl, A. Smith, and N. Pryds, “Comparison of adjustable permanent magnetic field sources,” *Journal of Magnetism and Magnetic Materials*, vol. 322, no. 22, pp. 3664–3671, 2010.

[32] R. Bjørk, C. Bahl, A. Smith, and N. Pryds, “Review and comparison of magnet designs for magnetic refrigeration,” *International Journal of Refrigeration*, vol. 33, no. 3, pp. 437–448, 2010.

[33] V. K. Pecharsky and K. A. Gschneidner Jr., “ $\text{Gd}_5(\text{SixGe}_{1-x})_4$: An Extremum Material,” *Advanced Materials*, vol. 13, no. 9, pp. 683–686, 2001.

[34] A. O. Pecharsky, K. A. Gschneidner, and V. K. Pecharsky, “The giant magnetocaloric effect of optimally prepared $\text{Gd}_5\text{Si}_2\text{Ge}_2$,” *Journal of Applied Physics*, vol. 93, pp. 4722–4728, 4 2003.

[35] Y. Mudryk, Y. Lee, T. Vogt, K. A. Gschneidner, and V. K. Pecharsky, “Polymorphism of $\text{Gd}_5\text{Si}_2\text{Ge}_2$: The equivalence of temperature, magnetic field, and chemical and hydrostatic pressures,” *Phys. Rev. B*, vol. 71, p. 174104, May 2005.

[36] R. Kiefe and J. S. Amaral, “FEMCE – A 3D finite element simulation tool for magnetic refrigerants,” *International Journal of Refrigeration*, vol. 173, pp. 180–184, 5 2025.

[37] C. S. Mejía, T. Niehoff, M. Straßheim, E. Bykov, Y. Skourski, J. Wosnitza, and T. Gottschall, “On the high-field characterization of magnetocaloric materials using pulsed magnetic fields,” *Journal of Physics: Energy*, vol. 5, p. 034006, 5 2023.

[38] C. O. Amorim, F. Mohseni, R. K. Dumas, V. S. Amaral, and J. S. Amaral, “A geometry-independent moment correction method for the MPMS3 SQUID-based magnetometer,” *Meas. Sci. Technol.*, vol. 32, p. 105602, 10 2021.

[39] J. S. Amaral and V. S. Amaral, “On estimating the magnetocaloric effect from magnetization measurements,” *Journal of Magnetism and Magnetic Materials*, vol. 322, pp. 1552–1557, 5 2010.

[40] S. Das, J. S. Amaral, and V. S. Amaral, “Handling mixed-state magnetization data for magnetocaloric studies—a solution to achieve realistic entropy behaviour,” *Journal of Physics D: Applied Physics*, vol. 43, p. 152002, mar 2010.

- [41] L. Caron, Z. Q. Ou, T. T. Nguyen, D. T. C. Thanh, O. Tegus, and E. Brück, “On the determination of the magnetic entropy change in materials with first-order transitions,” *Journal of Magnetism and Magnetic Materials*, vol. 321, pp. 3559–3566, 11 2009.
- [42] H. N. Bez, H. Yibole, A. Pathak, Y. Mudryk, and V. K. Pecharsky, “Best practices in evaluation of the magnetocaloric effect from bulk magnetization measurements,” *Journal of Magnetism and Magnetic Materials*, vol. 458, pp. 301–309, 7 2018.
- [43] A. Aharoni, “Demagnetizing factors for rectangular ferromagnetic prisms,” *J. Appl. Phys.*, vol. 83, pp. 3432–4, 1998.
- [44] A. Smith, K. K. Nielsen, D. V. Christensen, C. R. Bahl, R. Bjørk, and J. Hattel, “The demagnetizing field of a nonuniform rectangular prism,” *Journal of Applied Physics*, vol. 107, 5 2010.
- [45] D. V. Christensen, K. K. Nielsen, C. R. Bahl, and A. Smith, “Demagnetizing effects in stacked rectangular prisms,” *Journal of Physics D: Applied Physics*, vol. 44, p. 215004, 5 2011.
- [46] K. P. Skokov, V. V. Khovaly, K.-H. Müller, J. D. Moore, J. Liu, and O. Gutfleisch, “Magnetocaloric materials with first-order phase transition: thermal and magnetic hysteresis in $\text{LaFe}_{11.8}\text{Si}_{1.2}$ and $\text{Ni}_{2.21}\text{Mn}_{0.77}\text{Ga}_{1.02}$ (invited),” *Journal of Applied Physics*, vol. 111, p. 07A910, 02 2012.
- [47] A. Chirkova, K. Skokov, L. Schultz, N. Baranov, O. Gutfleisch, and T. Woodcock, “Giant adiabatic temperature change in FeRh alloys evidenced by direct measurements under cyclic conditions,” *Acta Materialia*, vol. 106, pp. 15–21, 2016.
- [48] F. Cugini and M. Solzi, “On the direct measurement of the adiabatic temperature change of magnetocaloric materials,” *Journal of Applied Physics*, vol. 127, p. 123901, 03 2020.
- [49] T. Gottschall, K. P. Skokov, B. Frincu, and O. Gutfleisch, “Large reversible magnetocaloric effect in Ni-Mn-In-Co,” *Applied Physics Letters*, vol. 106, p. 021901, 01 2015.
- [50] H. Zeng, J. Zhang, C. Kuang, and M. Yue, “Direct Measurements of Magneto-caloric Effect of $\text{Gd}_5\text{Si}_2\text{Ge}_2$ Alloys in Low Magnetic Field,” *Journal of Superconductivity and Novel Magnetism*, vol. 25, pp. 487–490, 2012.
- [51] T. Gottschall, K. P. Skokov, M. Fries, A. Taubel, I. Radulov, F. Scheibel, D. Benke, S. Riegg, and O. Gutfleisch, “Making a Cool Choice: The Materials Library of Magnetic Refrigeration,” *Advanced Energy Materials*, vol. 9, no. 34, p. 1901322, 2019.
- [52] K. Wang, M. Zhang, Y. Ouyang, J. Liu, and H. Zhang, “Enhancement of rotating magnetocaloric effect by Fe substitution in $\text{NdCo}_{5-x}\text{Fe}_x$ alloys,” *Intermetallics*, vol. 118, p. 106676, 2020.
- [53] A. Gschneidner, V. K. Pecharsky, and A. O. Tsokol, “Recent developments in magnetocaloric materials,” *Rep. Prog. Phys.*, vol. 68, pp. 1479–539, 6 2005.
- [54] J. Y. Law and V. Franco, “Pushing the limits of magnetocaloric high-entropy alloys,” *APL Materials*, vol. 9, p. 080702, 08 2021.
- [55] L. D. Griffith, Y. Mudryk, J. Slaughter, and V. K. Pecharsky, “Material-based figure of merit for caloric materials,” *Journal of Applied Physics*, vol. 123, p. 034902, 01 2018.